Analytical and Bioanalytical Chemistry (2019) 411:603–616
https://doi.org/10.1007/s00216-018-1362-6

RESEARCH PAPER

A versatile quantitative microdroplet elemental imaging method optimised for integration in biochemical workflows for low-volume samples

Kai Kysenius[1,2] · Bence Paul[3,4] · James B. Hilton[1] · Jeffrey R. Liddell[1] · Dominic J. Hare[3,5,6,7] · Peter J. Crouch[1,2,7]

Received: 2 July 2018 / Revised: 18 August 2018 / Accepted: 4 September 2018 / Published online: 15 September 2018

Abstract

Laser ablation-inductively coupled plasma-mass spectrometry (LA-ICP-MS) analysis of μ-droplets is becoming an attractive alternative for detecting and quantifying elements in biological samples. With minimal sample preparation required and detection limits comparable to solution nebulisation ICP-MS, μ-droplets have substantial advantages over traditional elemental detection, particularly for low volumes, such as aliquots taken from samples required for multiple independent biochemical assays, or fluids and tissues where elements of interest exist at native concentrations not suited to the necessary dilution steps required for solution nebulisation ICP-MS. However, the characteristics of μ-droplet residue deposition are heavily dependent on the matrix, and potential effects on signal suppression or enhancement have not been fully characterised. We present a validated and flexible high-throughput method for quantification of elements in μ-droplets using LA-ICP-MS imaging and matrix-matched external calibrants. Imaging the entire μ-droplet area removes analytical uncertainty arising from the often-heterogenous distribution when compared to radial or bisecting line scans that capture only a small portion of the droplet residue. We examined the effects of common matrices found in a standard biochemistry workflow, including native protein and salt contents, as well as reagents used in typical preparation steps for concurrent biochemical assays, such as total protein quantification and enzyme activity assays. We found that matrix composition results in systemic, concentration-dependent signal enhancement and suppression for carbon, whereas high sodium content has a specific space-charge-like suppression effect on high masses. We confirmed the accuracy of our method using both a certified serum standard (Seronorm™ L1) and independent measurements of analysed samples by solution nebulisation ICP-MS, then tested the specificity and reproducibility by examining spinal cord tissue homogenates from SOD1-G93A transgenic mice with a known molecular phenotype of increased copper- and zinc-binding superoxide dismutase-1 expression and altered copper-to-zinc stoichiometry. The method presented is rapid and transferable to

Published in the topical collection *Elemental and Molecular Imaging by LA-ICP-MS* with guest editor Beatriz Fernández García.

Dominic J. Hare and Peter J. Crouch contributed equally to this work.

Electronic supplementary material The online version of this article (https://doi.org/10.1007/s00216-018-1362-6) contains supplementary material, which is available to authorized users.

✉ Kai Kysenius
kai.kysenius@unimelb.edu.au

[1] Department of Pharmacology and Therapeutics, The University of Melbourne, Parkville, Victoria 3052, Australia

[2] The Florey Institute of Neuroscience and Mental Health, 30 Royal Parade, Parkville, Victoria 3052, Australia

[3] Melbourne Dementia Research Centre at The Florey Institute of Neuroscience and Mental Health and The University of Melbourne, Parkville, Victoria 3052, Australia

[4] School of Earth Sciences, The University of Melbourne, Parkville, Victoria 3052, Australia

[5] Elemental Bio-imaging Facility, University of Technology Sydney, Broadway, Sydney, New South Wales 2007, Australia

[6] Department of Clinical Pathology, The University of Melbourne, Parkville, Victoria 3052, Australia

[7] Florey Department of Neuroscience and Mental Health, The University of Melbourne, Parkville, Victoria 3052, Australia

multiple other biological matrices and allows high-throughput analysis of low-volume samples with sensitivity comparable to standard solution nebulisation ICP-MS protocols.

Keywords Bioanalytical methods · Biological samples · Laser ablation · Mass spectrometry/ICP-MS · Trace elements · Metals/heavy metals

Introduction

The elemental composition of biological material is intimately linked to functionality. Covalently bound heteroatoms (e.g. sulphur, phosphorus, iodine) often dictate protein-ligand binding sites and biochemical activity [1, 2], while metal ions are thought to be associated with ~ 50% of all known enzymatic reactions [3], where they participate in a range of processes from stabilising net charge to acting as redox centres [4]. With such a diverse number of biological functions, it is not surprising that changes in endogenous elemental concentrations have been associated with numerous pathologies and are considered promising therapeutic targets for neurodegenerative diseases [5], cancer [6], and a number of other chronic health conditions. Further, exogenous elements are regularly used in clinical practice, such as platinum-containing anti-cancer drugs [7] and imaging contrast agents [8], both of which have harmful antecedent effects.

Accurate and precise determination of elemental composition is paramount to understanding how often subtle variations are involved in disease processes. Traditionally, this has been performed using conventional atomic spectrometry techniques, or inductively coupled plasma-mass spectrometry (ICP-MS). While ICP-MS is well-suited to many biological applications, it does have several limitations. These include often extensive sample preparation for solid samples (e.g. microwave digestion, lyophilisation), the need to dilute low-volume samples for use with typical sample introduction systems, difficulties in matrix-matching complex biological specimens, and the effects of incomplete polyatomic interference removal on detection limits for trace endogenous elements (e.g. selenium, iodine, cobalt). As such, potential contamination and/or insufficient sensitivity limits the applicability of solution nebulisation (SN-)ICP-MS for low-volume samples, particularly when starting material is also required for additional biochemical assays.

Laser ablation (LA-)ICP-MS offers a suitable alternative via its capacity for discrete sampling of the source material. In the absence of significant amounts of water and resulting need for the ICP to desolvate an aqueous solution, both spectral and matrix-based polyatomic interferences can be negated by optimising system conditions to reduce temperature (by lowering forward power), residence time of the analyte in the plasma (by decreasing sampling depth) [9], and the use of low flow rates of a reaction gas to remove a specific interfering species (e.g. H_2 for removal of spectral $^{40}Ar^{16}O^+$ interference on $^{56}Fe^+$) [10]. For biological samples, which are most often encountered on a silica glass mount, such as a microscope slide, laser energy fluence (that is, the energy distribution across the area on which the beam is focused; in J cm^{-2}) can also be optimised to ensure complete ablation of the sample while not surpassing the energy threshold required for UV lasers to remove material from the underlying support [11]. Combined, these conditions are suitable for interference-free measurements of low-level analytes [12] and ideal for direct analysis of micro- and nanolitre volume samples.

Substantial attention has been paid to the utility of LA-ICP-MS for assessing the elemental composition of sample residues remaining after deposition and drying of microdroplets following the first reported example by Yang et al. in 2005 [13]. Here, 20-μL volumes of aqueous zinc, cadmium, selenium, and lead-containing standards and environmental/biological samples were deposited on a polystyrene substrate and dried, yielding concentrated residues of metal salts less than 500 μm in diameter. The high-throughput potential—originally put at ~ 250 samples per hour—has not been capitalised upon in the decade since, though proof-of-concept has been described in a range of biological applications [14–22].

The emergence of LA-ICP-MS imaging, and the challenges involved in obtaining absolute quantitative data that came with it [23], turned attention to micro (μ-)droplets as a simple method for external calibration [24] and isotope dilution [25] quantification (biological applications reviewed by Pozebon et al. [26, 27]). Most applications have used only representative bisecting lines of ablation through a standard deposited on a substrate, with a focus on imaging applications. As available imaging software tools have become more refined and user-friendly while also rapidly expanding data analysis capabilities [28–31], the potential to revisit high-throughput μ-droplet analysis that capitalises upon the advantages of fast LA-ICP-MS mapping becomes apparent. Spatial reconstructions of element distribution across the total area of μ-droplet residue removes uncertainty arising from non-uniform residue deposition, or 'coffee ring' effect [32].

We present here a detailed analytical assessment of imaging μ-droplets for quantification of elements in low-volume samples and highlight the versatility of this approach by applying it to a range of commonly encountered research settings that necessitate robust analytical methods for high-value samples.

Materials and methods

Standards and chemicals

Mixed-element standards were prepared using step dilution of a 500 μg L^{-1} certified multi-element standard for ICP-MS in 1% (*v*/*v*) HNO_3 (Agilent Technologies, Mulgrave, Australia) to 100 μg L^{-1}, 50 μg L^{-1}, 10 μg L^{-1}, and 5 μg L^{-1} in 1% (*v*/*v*) HNO_3 (from Suprapur®-grade 65% HNO_3 in ISO 3696 Grade 1 Milli-Q 18.2 MΩ cm water; both Merck Millipore, Bayswater, Australia). In-house prepared standards for matrix-matching were prepared from individual 1 M stock solutions of laboratory-grade metal salts (see Electronic Supplementary Material (ESM), Table S1) weighed using an Ohaus AX224 (Port Melbourne, Australia) analytical balance (precision = ± 0.0001 g; accurate to 82 mg). Salts were quantitatively transferred to metal-free 1.5-mL polypropylene vials (Techno Plas, St Marys, Australia) and made to volume (1 mL) in either Milli-Q water or analytical reagent-grade 37% (*w*/*w*) HCl (Merck Millipore) for $FeCl_2{\cdot}4H_2O$ to prevent Fe^{2+} autooxidation and Fe^{3+} precipitation when further diluted. A mixed-element 10 mM stock solution was then prepared in Milli-Q water. Working standards were prepared using serial dilution in Milli-Q water to give final estimated concentrations of 0 (matrix blank), 1 μM, 5 μM, 10 μM, 50 μM, 100 μM, 500 μM, 1 mM, and 5 mM. For matrix-matching experiments, mixed-element standards were prepared in Milli-Q water containing 3-*sn*-phosphatidylcholine (P1263), urea, NaCl, glucose, Triton X-100, or sodium dodecyl sulfate (SDS; all Sigma-Aldrich). Analytical performance of the optimised matrix-matching protocol was assessed using a 1 mg mL^{-1} bovine serum albumin (BSA; Sigma-Aldrich) and 1× Tris-buffered saline (TBS; 50 mM Tris-Cl, pH 7.6; 150 mM NaCl; Sigma-Aldrich; in Milli-Q H_2O) as the diluent for samples and standards. Accuracy was assessed using Seronorm™ Trace Elements Serum L1 (SERO, Billingstad, Norway; Ref, 201405; Lot, 1309438). The lyophilised standard was reconstituted in Milli-Q water per the supplier guidelines and used neat or diluted 1:10 and 1:40 in BSA-TBS.

Ethics approval statement and animal details

The use of biological material taken from wild-type C57/B6 and transgenic mice was approved by The University of Melbourne Animal Ethics Committee (approval number 1312908). All procedures were conducted in accordance with National Health and Medical Research Council guidelines.

Hemizygous mice expressing a transgene for human superoxide dismutase-1 (SOD1) containing the G93A substitution mutation ($SOD1^{G93A}$) on the mixed B6/SJL background were from the Jackson Laboratories (strain B6SJL-Tg(SOD1*G93A)1GurJ; Bar Harbor, USA) and generously provided by Prize4Life. Non-transgenic littermates were used as a control (Jackson Laboratories).

Preparation of spinal cord lysates

Mouse spinal cord lysates (Fig. 1(a)) were prepared by homogenising dissected tissue with polypropylene pestles in TBS containing 0.5% (*v*/*v*) phosphatase inhibitor cocktail 2 (Sigma-Aldrich), 2% (*v*/*v*) cOmplete™ EDTA-free protease inhibitor (Roche, Hawthorn, Australia), and 5% (*v*/*v*) DNAse I (Sigma-Aldrich). Homogenates were then separated into TBS-soluble and TBS-insoluble fractions by centrifugation

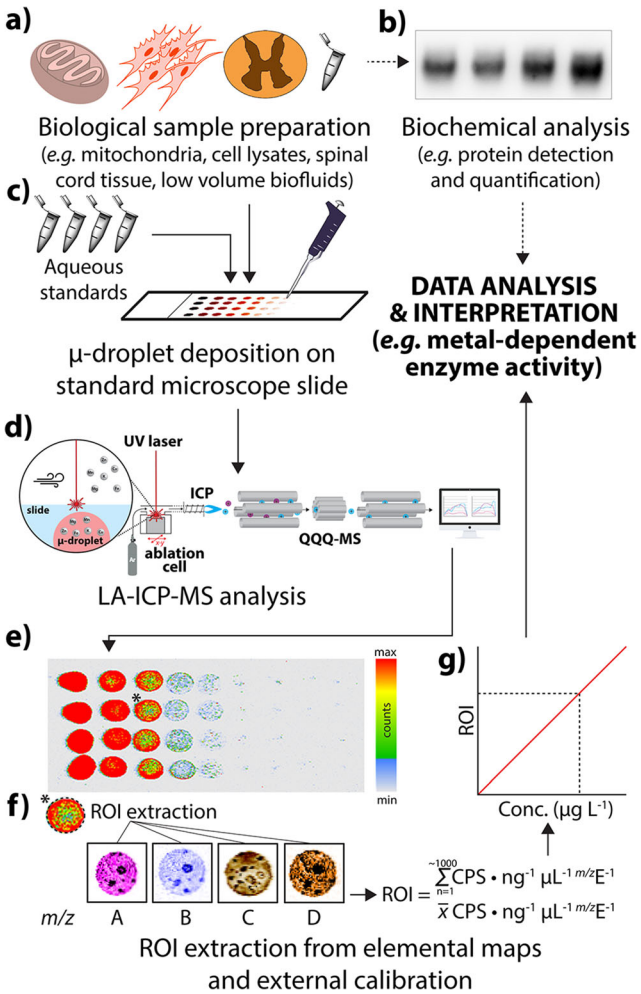

Fig. 1 Workflow for μ-droplet quantification of minor and trace elements in low-volume samples. (a) Solubilised preparations of biological matrices are aliquoted for LA-ICP-MS analysis and concurrent biochemical assays (b). (c) Neat or diluted samples are deposited using an air-displacement pipette onto a microscope slide alongside aqueous standards containing each analyte. Following air-drying and LA-ICP-MS analysis (d), where all deposited residue is ablated, images are constructed (e) and used to extract mean and total signal attributable to each element ($^{m/z}$E) deposited μ-droplet (f) and subsequent quantification via external calibration (g)

at 18,000×*g*, for 30 mins at 4 °C, and the TBS-soluble supernatant was transferred to a separate vial. At this point, aliquots for biochemical analysis can be taken (Fig. 1(b)).

Inductively coupled plasma-mass spectrometry

Concentrations of the investigated elements in standard solutions were confirmed using SN-ICP-MS. Aliquots of standards were diluted 1:10 in 1% (*v*/*v*) HNO_3 in 1.5-mL polypropylene vials (Techno Plas) and analysed using an Agilent Technologies 7700x ICP-MS with a MicroMist concentric nebuliser and Scott-type double-pass spray chamber (Glass Expansion, Port Melbourne, Australia). Yttrium ($m/z = 89$; Choice Analytical, Thornleigh, Australia) was used as an online internal standard, introduced via a Teflon T-piece. Helium (4 mL min^{-1}) was used as a collision gas. External calibration with mixed-element standards in 1% (*v*/*v*) HNO_3 (from TraceCERT® stock solutions in 10% (*v*/*v*) HNO_3; Sigma-Aldrich) was used to generate quantitative data using MassHunter software (rev. G7201B; Agilent Technologies).

The elemental composition of mouse spinal cord homogenates was determined using a method modified from Hilton et al. [33]. Briefly, homogenates were lyophilised overnight in a vacuum freeze dryer (Ezzi Vision, Chirnside Park, Australia), digested in 50 μL of 65% (*w*/*w*) HNO_3 at room temperature for ~2 h and then heated at 70 °C on a heating block for ~5 min, or until the solution was clear. Digests were diluted 1:20 with 1% (*v*/*v*) HNO_3 prior to analysis using the conditions above.

Microdroplet deposition

Droplets (1 μL) of samples and standards (Fig. 1(c)) were deposited onto silica glass microscope slides (Menzel-Gläser Superfrost® Plus; Thermo-Fisher Scientific, Scoresby, Australia) manually using a Gilson P2 air-displacement pipette (precision = ± 0.0025 μL; John Morris Group, Willoughby, Australia). The solution was partially dispensed as a droplet on the pipette tip, which was gently placed on the slide surface before being fully expelled. Standards and samples were deposited in rows within the 5 × 2.5 cm working area of a single slide and then air-dried in a particle-free environment overnight. Samples can feasibly be stored indefinitely in an airtight container; in this study, the maximum period between μ-droplet deposition and analysis was 5 days.

Laser ablation-inductively coupled plasma-mass spectrometry

Laser ablation-ICP-MS experiments were based on our previously reported method for μ-droplet analysis (Fig. 1(d)) [12] with additional modification for triple quadrupole ICP-(QQQ-)MS. Operating conditions are shown in Table S2 (see ESM). A NewWave Research NWR213 laser ablation system (Kennelec Scientific, Mitcham, Australia) with a standard two-volume cell was used for all analyses. Briefly, the ablation cell (10 × 10 cm) was loaded with a maximum of three microscope slides per analysis round. A scan region encompassing all microdroplet residues was established for each slide (roughly 5 × 2.5 cm; total area = 12.5 cm^2), over which lines of ablation spaced at 100-μm intervals were drawn. A square beam 100 μm wide scanned at 400 μm s^{-1} and 0.3 J cm^{-2} fluence was used to remove all deposited material while not ablating the supporting glass (minimum fluence threshold for ablation of silicate glass 2.4 J cm^{-2} [34]), resulting in a total analysis time of approximately 8–14 h per slide. Argon was used as the carrier gas (1.2 L min^{-1}).

All measurements were performed using an Agilent 8800 triple quadrupole ICP-(QQQ-)MS system with 'cs' lenses. The ICP-QQQ-MS system used was previously optimised to 'no gas' tuning parameters to maximise ion focusing and transmission via the Q2 ion-guide and collision/reaction cell [35]. The ICP-QQQ-MS system was configured to measure the mass-to-charge (*m/z*) ratios for elements listed in Table S2 (see ESM) in time-resolved analysis mode. Dwell time per mass was set to equate to four *m/z* readings per second, or a total integration time of 0.25 s per scan cycle [36].

Image generation and data analysis

Single line scans (as .csv files) were collated into hyperspectral images using *iolite* (v.3; The University of Melbourne, Parkville, Australia) [37] with the *Biolite* add-on for image analysis [28] (Fig. 1(e); see Hare et al. [38] for a visual tutorial). Modifications to the image analysis code were made using Igor Pro (v7; WaveMetrics, Inc., Portland, USA).

Contour plots of background signal intensity and drift for each measured *m/z* were interpolated from mean signal intensity in ~10 randomly positioned ~250-mm^2 areas containing no residue and used to correct for each μ-droplet. An elliptical region of interest (ROI) tool was used to extract mean ($\bar{x}$) counts per second (CPS) and total counts per second (Σ of ~1000 pixels) for each *m/z* from the complete μ-droplet area (Fig. 1(f)). External calibration was performed via nonlinear regression analysis using a log-log nonlinear model of a 9-point (including matrix blank) calibration curve in Prism (v7, GraphPad, La Jolla, USA). Limit of detection (LOD) and limit of quantification (LOQ) were calculated according to the 3σ and 10σ criteria, respectively, using the matrix blank. All μ-droplet dilution series were analysed in triplicate, or as otherwise stated. Recovery measurements are reported for only measured analytes >LOQ with Grubbs' test (1% stringency) applied to eliminate statistical outliers. All statistical testing was performed using *Biolite*, Excel 2016 (Microsoft Co., Redmond, USA), and Prism.

Results and discussion

Effects of μ-droplet matrix on element distribution

We examined the effect of matrix composition on heterogeneity of element deposition following evaporation of H_2O by comparing background ^{23}Na levels in 1-μL droplets of aqueous (as 1% (*v*/*v*) HNO_3), protein (BSA)- and salt (TBS)-rich vehicles, and mixed BSA-TBS representative of biological samples with minimal sample preparation, including two μ-droplets spiked with 100 pg μL^{-1} of a mixed-element standard including Na (Fig. 2a). Each sample preparation method led to distinct heterogenous analyte distribution in the remaining residues. For HNO_3, trace levels of endogenous elements were assumed to be below those deposited in concentrated areas at the centre of the circular droplet. For ^{23}Na, Tris-buffered saline containing 150 mM NaCl (equivalent to ~ 3.5 μg μL^{-1} Na) provided a fairly uniform distribution with punctate areas of higher signal intensity, including in the approximate centre of the droplet, whereas BSA contained lower background contaminant levels reminiscent of the 'coffee ring' effect observed in biological matrices deposited on a porous cellulose membrane [32] with an additional concentrated area at the centre. Heterogeneity in residue deposition can be attributed to a chromatographic-like effect with the proprietary silane-like slide surface acting as a stationary phase and the vehicle dispersing as a mobile phase while drying, resulting in diffusion of the μ-droplet over larger areas and potentially limiting sample throughput. Mixed BSA-TBS droplets showed a similar but more diffuse pattern with a broader 'ring' effect and dense inner edge. The BSA molecule has a general high affinity to divalent metals [39], and the presence at high concentrations may provide an additional matrix component that affixes mobilised elements within the area on which the μ-droplet was deposited. With the additional 100 pg mixed-element spike, analyte distribution was more uniform in the mixed TBS-BSA μ-droplet.

Addition of 100 pg μL^{-1} standard solution amplified the effects observed in matrix blanks. Histograms of signal intensity binned per 10-mm^2 area were used to assess the heterogeneity of each vehicle by measuring the difference between mean and median values for ^{7}Li, ^{13}C, and ^{63}Cu (Table 1; Fig.

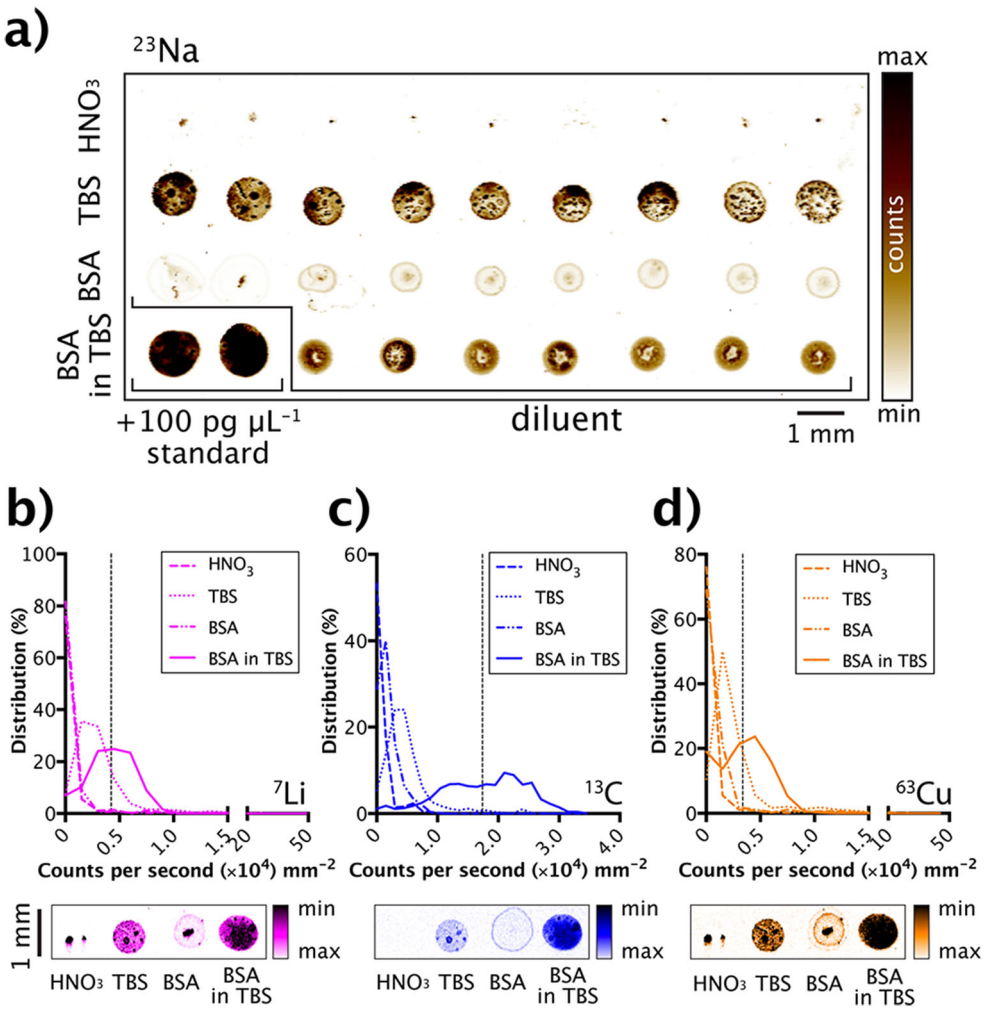

Fig. 2 Heterogeneity in residue deposition of dried μ-droplets. **a** Blank diluents had varying background levels of Na, including ~ 3.5 μg in TBS. Histograms of each preparation showed the smallest variance between median and mean (dashed vertical line) for mixed BSA-TBS vehicle (shown here as solid lines); hence, most homogenously distributed deposition of spiked **b** ^{7}Li, **c** ^{13}C, and **d** ^{63}Cu occurred with a mixed TBS-BSA vehicle

Table 1 Comparison of matrix effect on heterogeneity of analyte distribution (as median and mean signal intensities in counts per second [CPS] per 10 mm^2)

Diluent	*m/z*	Median (CPS)	Mean (CPS)	Mean/median difference (%)
HNO_3	7	0	15,284	100
	13	0	238	100
	63	0	12,673	100
TBS	7	2399	3007	20
	13	4024	4976	19
	63	1971	2771	29
BSA	7	131	7630	98
	13	1422	1718	17
	63	370	6094	94
BSA in TBS	7	4265	4224	− 1
	13	18,144	17,384	− 4
	63	3569	3367	− 6

2b–d). The smallest variance was observed in the mixed BSA-TBS diluent, where the difference between mean and median was 1–6%, compared to 17–100% for all other vehicles, primarily due to areas within the ROI where residue present was <LOD. These data suggest that certified multi-element standards in a simulated high-salt, high-protein biological matrix produce a homogeneous residue deposition and are suited for quantitative analysis with minimal intra-sample variability.

Limits of detection and quantification in simple-matrix diluents The LOD and LOQ for all measured analytes in matrix blank (1% (*v*/*v*) HNO_3) and BSA-TBS vehicles were calculated from the 3σ and 10σ of the signal intensity of seven replicates of preparation blanks (Table 2). For 1% (*v*/*v*) HNO_3, absolute LOD ranged from 0.02 to 12.18 pg. Detection limits were substantially higher for most elements in mixed TBS-BSA. The ~200-fold increase for ^{23}Na constitutes the background contribution of 3.45 μg Na. Absolute LOD ranged from 0.10 to 49.34 pg, with higher limits for typical protein constituents (^{31}P) and abundant metals (^{39}K, ^{43}Ca), whereas typical minor and trace elements were consistently < 15 pg. This is equivalent to ~ 10 μg L^{-1}, or parts per billion, which is adequate to detect most endogenous elements in biological samples with minimal preparation or dilution. The performance of the proposed method is comparable to the dried-droplet method published by Hsieh et al. [14], and encompasses several additional biologically relevant elements (e.g. Ca, P, Fe, Cr, Rb, Sr, and Mo) with the flexibility needed for low-volume samples, such as those required for multiple concurrent biochemical assays where dilution of small aliquots limits sensitivity for analytes at already low concentrations in the analysed sample, such as cerebrospinal fluid (CSF) [40]. Limits of analysis were also comparable to a pseudo-flow injection method for quantifying metals in CSF using size exclusion chromatography hyphenated to ICP-MS [41].

Analysis of prepared standard solutions by SN-ICP-MS

Concentrations of prepared standard solutions used for external calibration in μ-droplet analysis were confirmed using SN-ICP-MS. As stated above, endogenous element concentrations in biological samples vary from ultra-trace (defined as < 1 μg L^{-1}; e.g. Mn in CSF) [40] to 'minor' levels > 100 mg μL^{-1} (e.g. K in serum) [42]. Thus, a sufficiently broad dynamic range spanning four to five orders of magnitude is necessary for simultaneous quantification of target elements in biological samples. Having calculated the LOD, the prepared standards (ESM Table S1) were used to demonstrate and validate the use of custom-prepared standards for quantification of metals in a BSA-TBS matrix. The analyte concentrations in prepared standards were independently determined using SN-ICP-MS to account for possible contamination and imprecision in weighing of source materials (Table 3) [43] and used to test our LA-ICP-MS μ-droplet method. Using a concentrated stock of independently measured single-element standards to produce a mixed multi-element calibration with an appropriate concentration range allows for a simple dilution, avoiding potential error introduced through serial dilutions. While we report quantification results using six elements with high relevance to biochemistry, the same approach can be used for any other water-soluble inorganic analyte.

Linearity and calibration curve obtained by LA-ICP-MS for imaging of μ-droplets

A log-log nonlinear model was fitted to summed signal intensity for each deposited μ-droplet of spiked mixed salt solutions in BSA-TBS for logistic regression analysis using Eq. 1 ($n = 4$ replicates; Fig. 3a–e):

$$\sum \mathrm{CPS}\ \mathrm{ng}^{-1}\mu\mathrm{g}^{-1} = 10^{(m\log[E])} + b \quad (1)$$

Table 2 Absolute LOD and LOQ values calculated for 1-μL droplets of 1% (*v*/*v*) HNO_3 and BSA-TBS matrix blanks

Element	1% (*v*/*v*) HNO_3		BSA-TBS		Ratio BSA-TBS:1% (*v*/*v*) HNO_3
	LOD (pg)	LOQ (pg)	LOD (pg)	LOQ (pg)	
^{7}Li	0.02	0.08	0.33	1.09	14.1
^{23}Na	0.11	0.35	23.6	78.5	221.5
^{24}Mg	5.29	17.6	35.8	119	6.8
^{27}Al	5.43	18.1	13.1	43.7	2.4
^{31}P	10.91	36.4	47.0	157	4.3
^{39}K	2.41	8.02	49.3	164	20.5
^{43}Ca	3.17	10.6	25.4	84.7	8.0
^{47}Ti	12.2	40.6	11.7	39.0	1.0
^{52}Cr	0.45	1.49	1.58	5.26	3.5
^{55}Mn	0.21	0.70	0.89	2.96	4.2
^{56}Fe	4.15	13.8	10.2	33.8	2.4
^{59}Co	0.10	0.32	0.08	0.26	0.8
^{60}Ni	0.71	2.37	10.2	33.9	14.3
^{63}Cu	0.10	0.34	2.55	8.50	25.3
^{66}Zn	0.07	0.24	2.88	9.59	40.1
^{78}Se	0.30	1.00	1.50	4.99	5.0
^{85}Rb	0.18	0.61	0.75	2.50	4.1
^{88}Sr	0.08	0.25	3.51	11.7	46.7
^{95}Mo	0.04	0.15	0.81	2.69	18.3
^{101}Ru	0.02	0.07	0.10	0.32	4.6
^{111}Cd	0.25	0.83	0.48	1.58	1.9
^{208}Pb	0.02	0.07	0.06	0.18	2.6

where Σ CPS ng^{-1} μL^{-1} is the sum of all counts per second attributable to element (*E*) within the bounds of the μ-droplet, *m* is the slope, and *b* is the *y*-intercept [44]. Using the minimum standard concentration greater than the calculated LOD for each prepared standard deposited (for all measured elements other than ^{24}Mg and ^{39}K) [45], we assessed linearity of calibration curves and the respective dynamic range (Table 4).

Polyatomic interferences

As spectral and matrix-based interferences are low in the conditions used [12], the LOD values are attributable to intrinsic instrumental noise. Interference formation for an acidified vehicle in the absence of comparable salt and protein contents, using the imaging conditions here, has been previously reported to be negligible [12]. To further support the previous

Table 3 Predicted and determined concentrations of elements in standard solutions by SN-ICP-MS

Nominal concentration	^{24}Mg		^{39}K		^{55}Mn		^{56}Fe		^{63}Cu		^{66}Zn	
	Predicted	Measured	Predicted	Measured	Predicted	Measured	Predicted	Measured	Predicted	Measured	Predicted	Measured
5 μM	122[a]	107[a]	196[a]	46.0[a]	275[a]	258[a]	279[a]	253[a]	318[a]	233[a]	327[a]	233[a]
10 μM	243[a]	203[a]	391[a]	164[a]	549[a]	513[a]	559[a]	514[a]	636[a]	461[a]	654[a]	461[a]
50 μM	1.22[b]	1.36[b]	1.96[b]	0.865[b]	2.78[b]	2.88[b]	2.79[b]	2.84[b]	3.18[b]	2.60[b]	3.27[b]	2.60[b]
100 μM	2.43[b]	2.38[b]	3.91[b]	3.64[b]	5.49[b]	5.14[b]	5.59[b]	5.17[b]	6.36[b]	4.66[a]	6.57[b]	4.66[b]
500 μM	12.2[b]	12.4[b]	19.6[b]	18.5[b]	27.5[b]	28.1[b]	27.9[b]	27.4[b]	31.8[b]	25.2[b]	32.7[b]	25.2[b]
1 mM	24.3[b]	24.4[b]	39.1[b]	37.3[b]	54.9[b]	55.7[b]	55.9[b]	55.1[b]	63.6[b]	49.8[b]	65.4[b]	68.5[b]

[a] $\mu g\ L^{-1}$. [b] $mg\ L^{-1}$

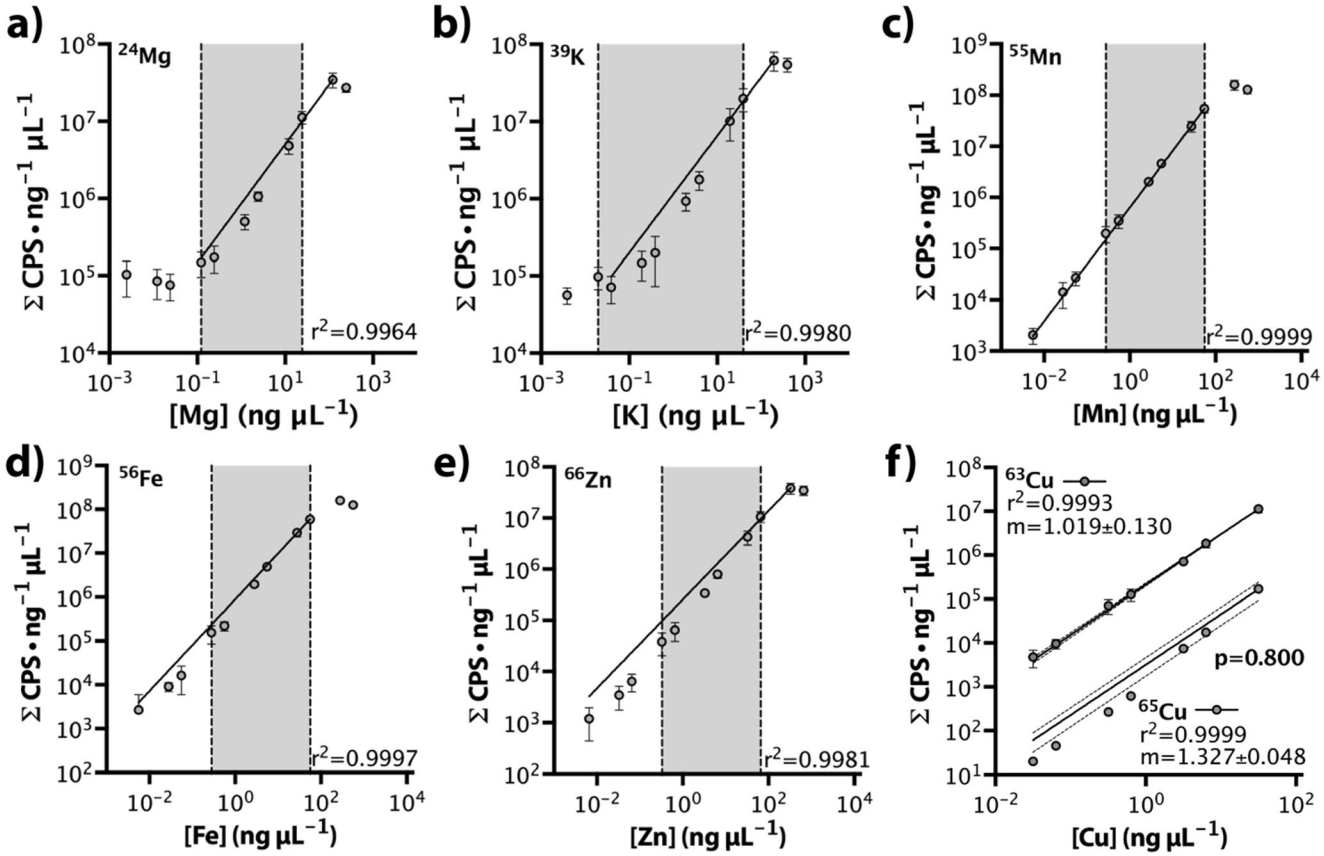

Fig. 3 Log-log nonlinear logistic regression analysis from µ-droplet analysis for **a** ^{24}Mg, **b** ^{39}K, **c** ^{55}Mn, **d** ^{56}Fe, and **e** ^{66}Zn standard solutions of metal salts. Grey area denoted upper and lower calibration range for SN-ICP-MS confirmation of in-house prepared standards. **f** Comparison of nonlinear logistic regression analysis of ^{63}Cu and ^{65}Cu, showing good linearity (0.9993 and 0.9999, respectively) and no significant difference in slope (m; $p = 0.800$; extra-sum-of-squares F test)

assertion, we examined the primary matrix-based interference expected in a biological specimen arising from $^{40}Ar^{23}Na^{+}$, $^{31}P^{16}O_2{}^{+}$, $^{36}Ar^{12}C^{14}N^{1}H^{+}$, and $^{16}O^{12}C^{35}Cl^{+}$ on ^{63}Cu [46]. We monitored both *m/z* 63 and *m/z* 65, representing the two stable Cu isotopes (natural abundance 69.15% and 30.85%, respectively) and compared the slopes, which showed good agreement ($p = 0.800$, extra-sum-of-squares F test, $F = 0.067$, df = 11; Fig. 3f) and an absolute LOD of 2.55 pg Cu. Within the dynamic range achieved and in physiologically relevant conditions, using ion focusing optimised for ICP-QQQ-MS [35], matrix-based interferences do not restrict LA-ICP-MS analysis in biochemical applications.

Effects of a simulated biological matrix on measurements

To further characterise the contribution of additional matrix constituents common to biochemical samples on method accuracy, 50 pg µL^{-1} multi-element standards with increasing concentrations of protein (as BSA), lipids (as mixed phosphatidylcholines),

Table 4 Correlation coefficient and dynamic range of $n = 8$–10 point nonlinear logistic regression analysis of LA-ICP-MS µ-droplet external calibration with spiked standards in a BSA-TBS vehicle

Element	Correlation coefficient (r^2)	Dynamic range (µL^{-1})
^{24}Mg	0.9964	5 µM–5 mM (122 µg–122 mg)
^{39}K	0.9980	5 µM–5 mM (195 µg–195 mg)
^{55}Mn	0.9999	100 nM–1 mM (5.49 ng–54.9 mg)
^{56}Fe	0.9997	100 nM–1 mM (5.58 ng–55.8 mg)
$^{63/65}$Cu	0.9993[a], 0.9999[b]	100 nM–1 mM (6.35 ng–63.5 mg)
^{66}Zn	0.9981	100 nM–1 mM (6.54 ng–65.4 mg)

[a] As ^{63}Cu. [b] As ^{65}Cu

urea ($CO(NH_2)_2$), salts (as NaCl), and glucose ($C_6H_{12}O_6$), as well as anionic (as sodium dodecyl sulfate) and nonionic (as Triton X-100) surfactants, commonly used in extraction buffers to permeabilise cell membranes (Fig. 4a–g) were analysed and mean signal intensities of lithium (*m/z* 7), copper (*m/z* 63), and lead (*m/z* 208) compared to the lowest tested matrix concentration ($n = 3$; one-way ANOVA with Dunnett's post hoc test for multiple comparisons). Concentrations were selected based on typical sample preparation and extraction buffers used in routine biochemistry protocols, with increasing amounts of organic matrix components showing the expected increase in mean *m/z* 13 signal intensity (Fig. 4h), while phospholipids reflective of neurological material increased the *m/z* 31 signal an order of magnitude higher than *m/z* 13, with higher signal-to-noise and equivalent variance over three replicate measurements (Fig. 4i). Carbon content generally resulted in a systematic suppression of signal intensity across a broad *m/z* range, while high sodium levels suppressed *m/z* 208 signal only.

When compared to the lowest matrix concentration, all biochemical matrix simulants induced statistically significant signal enhancement or suppression effects, depending on the primary matrix constituent. In contrast to the carbon enhancement effect observed for liquid matrices with a high organic component [47], which can be attributed to effects on plasma conditions specific to nebulisation and the substantially greater carbon load [48], a matrix concentration-dependent suppression of signal intensity at low (*m/z* 7), mid (*m/z* 65), and high (*m/z* 208) masses was not observed. While the concentrations tested were selected on the basis of common biological samples and were thus not sufficiently broad to fully characterise specific matrix effects of differing organic source material across a wide range, the results taken together suggest that respective analytes signal enhancement and suppression caused by carbon at low and high concentrations encountered in SN-ICP-MS (see Wiltsche et al. [48] and the references therein) also occurs in the dry plasma and lower carbon load as in the case of LA-ICP-MS. Mean signal intensities were generally an order of magnitude higher for each measured *m/z* in the presence of low amounts of carbon: ~ 30 μg for BSA, 60 μg for urea, 72 μg for glucose, and 2.9 μg for Triton X-100; 7 mg for the representative lipid 1-oleoyl-2-palmitoyl-phosphatidylcholine; and 5 mg for SDS (ESM Fig. S1).

For NaCl, the specific suppression of *m/z* 208 signal intensity is likely an effect of an inverse space-charge effect, which typically occurs due to ion beam defocussing of low-mass analytes by high-mass matrix components with greater kinetic energy [49]. In this case, the zone model of ion density [50] states that ^{23}Na focusing is highest closer to the torch and diffuses across the surface of the sampling cone, which likely impedes transmission of higher-mass $^{208}Pb^+$ ions that

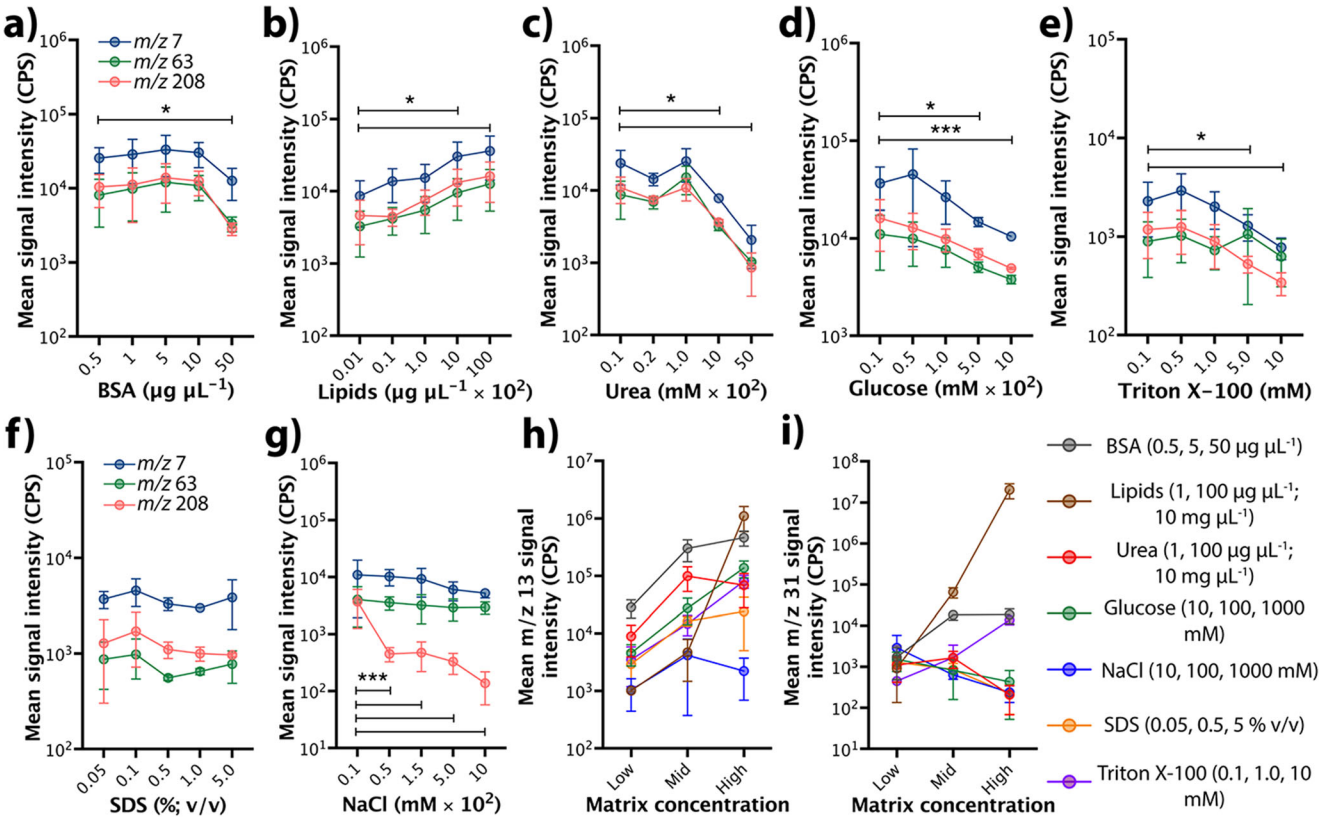

Fig. 4 Mean signal intensity for *m/z* 7, 63, and 208 (**a**–**g**); 13 (**h**); and 31 (**i**) in a deposited 1-μL droplet containing 50 pg Li, Cu, and Pb, and increasing concentrations of simulated biological matrices

ordinarily reach peak density in the cooler analytical zone of the plasma closer to the cone orifice. Additionally, the shorter sampling depth used in LA-ICP-MS in the present study further biases transmission against high-mass in favour of mid-mass elements.

Carbon and phosphorus contents of the matrix have implications for potential use of either ^{13}C or ^{31}P as an internal standard. While repeated standard measurements and variable background subtraction in *Biolite* give more confidence in correcting signal drift in LA-ICP-MS imaging applications as previously observed [28], the homogenous deposition (Fig. 1(a)) and superior signal-to-noise of ^{31}P could potentially be employed as an alternative to ^{13}C for μ-droplet analysis, though several of the limitations observed for ^{13}C are likely to also be encountered [51–53].

Droplet areas were consistently within a 4.5–6-mm^2 range for each tested matrix constituent with the exception of 0.1% (*v*/*v*) Triton X-100, which expanded to > 30 mm^2. The increased area covered by μ-droplet residue from extraction buffers at low concentrations may be attributable to the previously observed chromatographic-like diffusion expanding radially from the droplet centre as a result of reduced interactions between the non-polar hydrocarbon and organosilane coating of Superfrost® Plus slides. For SDS, the anionic organosulfate electrostatically likely interacts with the protonated amine group of the silanised slide to limit spread of the μ-droplet residue while drying. Reduced sample throughput due to the larger scanning areas needed for samples containing Triton X-100 at 0.1–1% (*v*/*v*) may be necessary, however, to offset the suppression of signal intensity for low-level analytes by the high carbon content of typical SDS preparations.

Accuracy of μ-droplet quantification

Trueness and precision were assessed using Seronorm™ Trace Element Serum L1 certified human serum standard reference material (Sero, Billingstad, Norway) according to ISO 5725-1 guidelines for determining method accuracy [54]. Percentage recoveries for certified concentration were also used to inspect possible matrix-specific effects of the Seronorm™ standard by quantifying elemental content in reconstituted lyophilised serum in Milli-Q water, and serum diluted in 1 μg L^{-1} BSA-TBS. External calibration was performed using matrix-matched mixed-element standards (0 ng μL^{-1}, 10 ng μL^{-1}, 20 ng μL^{-1}, and 100 ng μL^{-1} in BSA-TBS). Heterogeneous residue deposition deemed undiluted Seronorm™ unsuitable for analysis. Total protein concentration measured by spectrophotometry (using a NanoDrop™ UV-Vis spectrophotometer from ThermoFisher Scientific) was 8.3 μg μL^{-1} (1:10) and 3.2 μg μL^{-1} (1:40), indicating the total protein content (~ 83 μg) of undiluted standard would confer similar signal suppression effects as those shown in Fig. 4a. All elements were below LOQ in the 1:40 dilution, while lithium, iron, copper, zinc, and selenium were higher in the 1:10 dilution and were used to calculate percentage recovery, 95% confidence intervals, and intra- and inter-day variations (σ) over a 3-day period (Table 5). Recoveries ranged from 90.3% (Fe) to 97.7% (lithium), with 95% confidence intervals falling within the reference analytical uncertainty. The intra- and inter-day variance was under 10% for all measurements other than inter-day variance of 13.4% for lithium.

Application to a transgenic mouse model of metal dysregulation

The utility of the optimised and validated method was demonstrated by analysing spinal cord tissue from SOD1-G93A transgenic mice and non-transgenic controls. Wild-type SOD1 is an important antioxidant enzyme which requires equimolar binding of one copper and one zinc per protein subunit for physiological function. Mutations in the protein cause a familial form of the fatal neurodegenerative disorder amyotrophic lateral sclerosis (ALS), and transgenic expression of mutant SOD1 in mice accurately recapitulates the disease. Overexpression of SOD1-G93A in mice causes the protein to accumulate in the cytosol in a zinc-containing, copper-deficient form [55].

Zinc and copper, as the two metal ions associated with SOD1, and magnesium as a representative metal unaffected by altered SOD1 expression were determined using deposited μ-droplets of TBS-soluble and TBS-insoluble fractions from SOD1-G93A and non-transgenic mouse spinal cord tissue.

Table 5 Trueness and precision measures for Seronorm™ L1 diluted in 1:10 in 1 μg L^{-1} BSA-TBS

Element	Reference concentration (μg L^{-1})	Reference 95% CI	Measured concentration (μg L^{-1})	Measured 95% CI	% recovery	Intra-day σ (%)	Inter-day σ (%)
Li	5261	4202–6320	5139	4667–5611	97.7	1.2	13.4
Fe	1470	1170–1770	1328	1229–1426	90.3	5.1	8.4
Cu	1066	852–1281	1115	1043–1188	104.6	5.0	8.3
Zn	1057	844–1269	1022	978–1067	96.7	3.2	5.3
Se	86	51–120	105.6	99.6–111.8	122.9	9.6	0.9

Parallel SN-ICP-MS analysis of total metal levels in tissue homogenates was used as a reference method to assess specificity and reproducibility in biological samples with a characterised copper-specific molecular phenotype (Fig. 5).

The SOD1-G93A mice used have 25 copies of the mutant SOD1 transgene [56], resulting in substantially higher SOD1 protein levels when compared to than non-transgenic littermate controls expressing endogenous SOD1. Accordingly, zinc levels were elevated relative to controls, measured using both SN-ICP-MS and μ-droplet LA-ICP-MS quantifications (Fig. 5a). The increase in copper was less marked in the TBS-soluble fraction of SOD1-G93A mice ($p < 0.05$) and not statistically significant in either TBS-insoluble fractions or the total copper levels in the homogenates (Fig. 5b). This reflects the change in zinc:copper stoichiometry previously reported in transgenic mice expressing mutant SOD1 [33, 57, 58]. No change in magnesium levels, which are independent of the SOD1 protein, was detected (Fig. 5c).

Advantages and limitations of a μ-droplet quantification method

Accurate and precision determination of elemental concentrations in low-volume samples has a range of advantages in biochemical research and potential clinical use. The primary driver for developing this μ-droplet quantification method was the rapidly increasing appreciation for the importance of measuring bio-elements as part of larger biochemistry workflows, where each assay contributes to a broad and comprehensive assessment of the multifaceted properties of low-level inorganic species in a biological system. In a clinical setting, analysing CSF is one of the few accessible means to examine pathology of neurological disorders within the central nervous system [59]. The volume of fluid obtained from lumbar puncture is measured at the bedside as 'drops', determined to contain 60 μL of CSF using a remarkably similar 'matrix-matching' approach to roughly mimic pressure and fluid consistency, of which three 'drops', or 180 μL is the minimum volume needed for routine clinical biochemistry assays, such as glucose levels [60]. For high-abundance metals such as potassium, a dilution factor as low as 10 is necessary for measurements sufficiently higher than the method limit of quantification [42]. Elements present at lower physiological concentrations such as copper, with a reported mean concentration in undiluted CSF from 42 aged control subjects of 4.1 ± 0.1 pg μL^{-1} [61], would require c.a. 100 μL of CSF for routine SN-ICP-MS to produce a sufficient final volume for analysis using our previously described method for multi-element analysis [42, 62]. Using one-hundredth, the volume of CSF to achieve equivalent analytical performance thus has minimal impact on the total CSF sample volume available for other biochemical assays.

Some analytical limitations are shared between typical SN-ICP-MS and μ-droplet quantifications, specifically sensitivity for ultra-trace elements, including toxicants such as lead or essential metals like cobalt. Though reported lead concentrations in normal CSF vary from 0.32 pg μL^{-1} (median of $n = 56$) [63] to 1.3 ± 0.5 fg μL^{-1} (mean ± SD of $n = 42$) [61], our absolute quantification limit in a simulated CSF matrix for lead of 0.18 pg, at the upper end of this range, would be insufficient for robust quantification. It is noteworthy, however, that in the two studies reported, lead levels were either at or

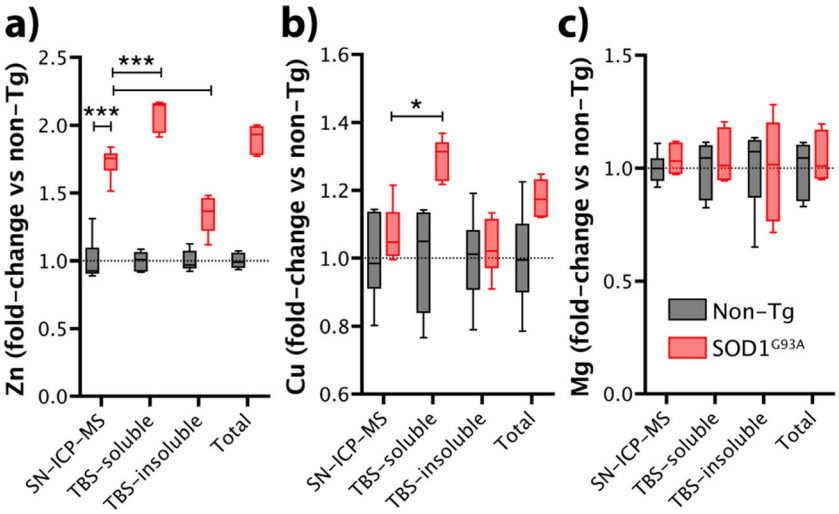

Fig. 5 **a**–**c** Specificity of zinc, copper, and magnesium in transgenic mice overexpressing copper- and zinc-binding SOD1 using SN-ICP-MS of tissue homogenates and LA-ICP-MS for μ-droplet analysis of TBS-soluble and TBS-insoluble fractions, as well as the combined total metal levels. Increased copper and zinc were most marked in the TBS-soluble fraction of spinal cord tissue homogenates of SOD1-G93A-overexpressing mice, where the highest concentrations of SOD1 are found (one-way ANOVA, $*p < 0.05$, $***p < 0.001$). Magnesium levels, which are not associated with mutation to SOD1, remained unchanged

below limits of quantification. Maass et al. [61] used a one-in-four dilution of an undefined volume of CSF aliquoted from a 10-mL original sample, whereas Gerhardsson and colleagues [63] did not specify the dilution factor used, instead referring to a method for analysis of blood and plasma [64]. Assuming a one-in-ten dilution optimised for multi-element quantification in plasma was used, this approach reported a distribution of CSF lead levels that fell below the 0.07 pg μL^{-1} limit of detection. Thus, the sensitivity of LA-ICP-MS imaging and this μ-droplet method allows for multi-element analysis in undiluted, low-volume samples, concentrated in a defined area for total consumption analysis.

The proposed μ-droplet quantification method for measuring element concentration in low-volume samples allows analysis of roughly 200–300 samples in 24 h and is applicable to virtually any biological sample with minimal sample preparation. This method is immediately transferable to new LA-ICP-MS technology incorporating fast imaging and high resolution [65, 66], providing sample throughput comparable to routine SN-ICP-MS protocols.

Though sample preparation is less demanding than normally required for SN-ICP-MS, manual deposition of the droplets using air-displacement pipettes creates a bottleneck that could be overcome by automated deposition, similar to those used for applying matrices to samples for matrix-assisted laser desorption/ionisation (MALDI). Automation of droplet deposition would also eliminate operator-dependent variation and ultimately improve precision. Modified thermal inkjet printers have been used to deposit picolitre volumes with precision < 10% [67, 68], and if used at the conditions of the present method, they could further decrease the amount of sample required for analysis.

Conclusions

A method for quantification of elements in μ-droplets by LA-ICP-MS was developed. This versatile method where sample matrix can be matched with relative ease can be readily integrated into standard biochemical laboratory practice where total element concentration is a necessary measured outcome. The primary advantage is the capacity to accurately and precisely detect elements in low-volume samples, reducing the burden on experiments where multiple independent analyses are required and minimal amounts of biological material are available.

Acknowledgements KK was a recipient of the Sigrid Juselius Foundation Postdoctoral Fellowship (Finland). DJH is a NHMRC Career Development Fellow (CDF1) - Industry (1122981) with Agilent Technologies. PJC is an NHMRC Career Development Fellow (CDF2 - 1084927). We wish to the Prize4Life Organization for providing experimental transgenic mice. The Florey Institute of Neuroscience and Mental Health acknowledge the strong support from the Victorian Government and the funding from the Operational Infrastructure Support Grant.

Author contributions Peter J Crouch and Kai Kysenius designed the project, prepared the samples, and edited the manuscript. Kai Kysenius performed the analyses, prepared the figures, and wrote the manuscript. James B Hilton and Jeffrey R Liddell prepared the samples and edited the manuscript. Dominic J Hare performed the SN-ICP-MS analysis and edited the manuscript. Bence Paul wrote the Iolite analysis code and edited the manuscript.

Funding information This study received support from the Jenny Barr Smith, Betty Laidlaw, and Jenny Simko Research Grants from the MND Research Institute of Australia.

Compliance with ethical standards

The use of biological material taken from wild-type C57/B6 and transgenic mice was approved by The University of Melbourne Animal Ethics Committee (approval number 1312908). All procedures were conducted in accordance with National Health and Medical Research Council guidelines.

Conflict of interest statements Bence Paul receives part of his salary from the sales of the Iolite software. Dominic J Hare receives research and material support from Agilent Technologies through the National Health and Medical Research Career Development Fellowship program. Procypra Therapeutics LLC, Collaborative Medicinal Development LLC, and The University of Melbourne are engaged in development of new therapeutics for ALS using the transgenic animal described herein. The other authors declare that they have no conflict of interest.

References

1. Kinoshita K, Nakamura H. Identification of the ligand binding sites on the molecular surface of proteins. Protein Sci. 2005;14:711–8. https://doi.org/10.1110/ps.041080105.
2. del Sol A, del Mesa A, Pazos F, Valencia A. Automatic methods for predicting functionally important residues. J Mol Biol. 2003;326:1289–302. https://doi.org/10.1016/S0022-2836(02)01451-1.
3. Waldron KJ, Rutherford JC, Ford D, Robinson NJ. Metalloproteins and metal sensing. Nature. 2009;460:823–30. https://doi.org/10.1038/nature08300.
4. Andreini C, Bertini I, Cavallaro G, Holliday GL, Thornton JM. Metal ions in biological catalysis: from enzyme databases to general principles. JBIC J Biol Inorg Chem. 2008;13:1205–18. https://doi.org/10.1007/s00775-008-0404-5.
5. Barnham KJ, Bush AI. Biological metals and metal-targeting compounds in major neurodegenerative diseases. Chem Soc Rev. 2014;43:6727–49. https://doi.org/10.1039/C4CS00138A.
6. Fouani L, Menezes SV, Paulson M, Richardson DR, Kovacevic Z. Metals and metastasis: exploiting the role of metals in cancer metastasis to develop novel anti-metastatic agents. Pharmacol Res. 2017;115:275–87. https://doi.org/10.1016/j.phrs.2016.12.001.
7. Michalke B. Platinum speciation used for elucidating activation or inhibition of Pt-containing anti-cancer drugs. J Trace Elem Med Biol. 2010;24:69–77. https://doi.org/10.1016/j.jtemb.2010.01.006.
8. Geraldes CFGC, Laurent S. Classification and basic properties of contrast agents for magnetic resonance imaging. Contrast Media Mol Imaging. 2009;4:1–23. https://doi.org/10.1002/cmmi.265.
9. Zhu G, Browner FR. Investigation of experimental parameters with a quadrupole ICP/MS. Appl Spectrosc. 1987;41

10. Lear J, Hare DJ, Fryer F, Adlard PA, Finkelstein DI, Doble PA. High-resolution elemental bioimaging of Ca, Mn, Fe, Co, Cu, and Zn employing LA-ICP-MS and hydrogen reaction gas. Anal Chem. 2012;84:6707–14. https://doi.org/10.1021/ac301156f.
11. Dyer PE, Karnakis DM, Key PH, Monk P. Excimer laser ablation for micro-machining: geometric effects. In: Fogarassy E, Geohegan D, Stuke M, editors. Laser ablation. Elsevier; 1996.
12. Hare DJ, Fryer F, Paul B, Bishop DP, Doble PA. Characterisation of matrix-based polyatomic interference formation in laser ablation-inductively coupled plasma-mass spectrometry using dried microdroplet ablation and its relevance for bioimaging. Anal Methods. 2016;8:7552–6. https://doi.org/10.1039/C6AY02545E.
13. Yang L, Sturgeon RE, Mester Z. Quantitation of trace metals in liquid samples by dried-droplet laser ablation inductively coupled plasma mass spectrometry. Anal Chem. 2005;77:2971–7. https://doi.org/10.1021/ac048275a.
14. Hsieh HF, Chang WS, Hsieh YK, Wang CF. Using dried-droplet laser ablation inductively coupled plasma mass spectrometry to quantify multiple elements in whole blood. Anal Chim Acta. 2011;699:6–10. https://doi.org/10.1016/j.aca.2011.05.002.
15. Hsieh HF, Chang WS, Hsieh YK, Wang CF. Lead determination in whole blood by laser ablation coupled with inductively coupled plasma mass spectrometry. Talanta. 2009;79:183–8. https://doi.org/10.1016/j.talanta.2009.03.027.
16. Nischkauer W, Vanhaecke F, Limbeck A. Self-aliquoting microgrooves in combination with laser ablation-ICP-mass spectrometry for the analysis of challenging liquids: quantification of lead in whole blood. Anal Bioanal Chem. 2016;408:5671–6. https://doi.org/10.1007/s00216-016-9717-3.
17. Cizdziel JV. Determination of lead in blood by laser ablation ICP-TOF-MS analysis of blood spotted and dried on filter paper: a feasibility study. Anal Bioanal Chem. 2007;388:603–11. https://doi.org/10.1007/s00216-007-1242-y.
18. Foltynova P, Kanicky V, Preisler J. Diode laser thermal vaporization inductively coupled plasma mass spectrometry. Anal Chem. 2012;84:2268–74. https://doi.org/10.1021/ac202884m.
19. Aramendia M, Rello L, Berail S, Donard A, Pecheyran C, Resano M. Direct analysis of dried blood spots by femtosecond-laser ablation-inductively coupled plasma-mass spectrometry. Feasibility of split-flow laser ablation for simultaneous trace element and isotopic analysis (vol 30, pg 296, 2015). J Anal At Spectrom. 2015;30:525. https://doi.org/10.1039/c4ja90069c.
20. Chantada-Vazquez MP, de Becerra-Sanchez C, Fernandez-del-Rio A, Sanchez-Gonzalez J, Bermejo AM, Bermejo-Barrera P, et al. Development and application of molecularly imprinted polymer - Mn-doped ZnS quantum dot fluorescent optosensing for cocaine screening in oral fluid and serum. Talanta. 2018;181:232–8. https://doi.org/10.1016/j.talanta.2018.01.017.
21. Kumtabtim U, Siripinyanond A, Auray-Blais C, Ntwari A, Becker JS. Analysis of trace metals in single droplet of urine by laser ablation inductively coupled plasma mass spectrometry. Int J Mass Spectrom. 2011;307:174–81. https://doi.org/10.1016/j.ijms.2011.01.030.
22. Chantada-Vázquez M, Moreda-Piñeiro J, Cantarero-Roldán A, Bermejo-Barrera P, Moreda-Piñeiro A. Development of dried serum spot sampling techniques for the assessment of trace elements in serum samples by LA-ICP-MS. Talanta. 2018;186:169–175. doi: https://doi.org/10.1016/j.talanta.2018.04.049.
23. Hare D, Austin C, Doble P. Quantification strategies for elemental imaging of biological samples using laser ablation-inductively coupled plasma-mass spectrometry. Analyst. 2012;137:1527–37. https://doi.org/10.1039/c2an15792f.
24. Pugh JAT, Cox AG, McLeod CW, Bunch J, Whitby B, Gordon B, et al. A novel calibration strategy for analysis and imaging of biological thin sections by laser ablation inductively coupled plasma mass spectrometry. J Anal At Spectrom. 2011;26:1667–73. https://doi.org/10.1039/C1JA10118H.
25. Moraleja I, Mena ML, Lázaro A, Neumann B, Tejedor A, Jakubowski N, et al. An approach for quantification of platinum distribution in tissues by LA-ICP-MS imaging using isotope dilution analysis. Talanta. 2018;178:166–71. https://doi.org/10.1016/j.talanta.2017.09.031.
26. Pozebon D, Scheffler GL, Dressler VL. Recent applications of laser ablation inductively coupled plasma mass spectrometry (LA-ICP-MS) for biological sample analysis: a follow-up review. J Anal At Spectrom. 2017;32:890–919. https://doi.org/10.1039/c7ja00026j.
27. Pozebon D, Scheffler GL, Dressler VL, Nunes MAG. Review of the applications of laser ablation inductively coupled plasma mass spectrometry (LA-ICP-MS) to the analysis of biological samples. J Anal At Spectrom. 2014;29:2204–28. https://doi.org/10.1039/c4ja00250d.
28. Paul B, Hare DJ, Bishop DP, Paton C, Nguyen VT, Cole N, et al. Visualising mouse neuroanatomy and function by metal distribution using laser ablation-inductively coupled plasma-mass spectrometry imaging (vol 6, pg 5383, 2015). Chem Sci. 2016;7:6576. https://doi.org/10.1039/c6sc90060g.
29. Paul B, Paton C, Norris A, Woodhead J, Hellstrom J, Hergt J, et al. CellSpace: a module for creating spatially registered laser ablation images within the Iolite freeware environment. J Anal At Spectrom. 2012;27:700–6. https://doi.org/10.1039/c2ja10383d.
30. Sforna MC, Lugli F. MapIT!: a simple and user-friendly MATLAB script to elaborate elemental distribution images from LA-ICP-MS data. J Anal At Spectrom. 2017;32:1035–43. https://doi.org/10.1039/c7ja00023e.
31. López-Fernández H, de Pessôa GS, Arruda MAZ, Capelo-Martínez JL, Fdez-Riverola F, Glez-Peña D, et al. LA-iMageS: a software for elemental distribution bioimaging using LA–ICP–MS data. J Cheminform. 2016;8:65. https://doi.org/10.1186/s13321-016-0178-7.
32. Nischkauer W, Vanhaecke F, Bernacchi S, Herwig C, Limbeck A. Radial line-scans as representative sampling strategy in dried-droplet laser ablation of liquid samples deposited on pre-cut filter paper disks. Spectrochim Acta Part B At Spectrosc. 2014;101:123–9. https://doi.org/10.1016/j.sab.2014.07.023.
33. Hilton JB, Mercer SW, Lim NK, Faux NG, Buncic G, Beckman JS, et al. Cu(II)(atsm) improves the neurological phenotype and survival of SOD1(G93A) mice and selectively increases enzymatically active SOD1 in the spinal cord. Sci Rep. 2017;7:42292. https://doi.org/10.1038/srep42292.
34. Grehn M, Seuthe T, Höfner M, Griga N, Theiss C, Mermillod-Blondin A, et al. Femtosecond-laser induced ablation of silicate glasses and the intrinsic dissociation energy. Opt Mater Express. 2014;4:689–700. https://doi.org/10.1364/ome.4.000689.
35. Bishop DP, Clases D, Fryer F, Williams E, Wilkins S, Hare DJ, et al. Elemental bio-imaging using laser ablation-triple quadrupole-ICP-MS. J Anal At Spectrom. 2016;31:197–202. https://doi.org/10.1039/c5ja00293a.
36. Lear J, Hare D, Adlard P, Finkelstein D, Doble P. Improving acquisition times of elemental bio-imaging for quadrupole-based LA-ICP-MS. J Anal At Spectrom. 2012;27:159–64. https://doi.org/10.1039/C1JA10301F.
37. Paton C, Hellstrom J, Paul B, Woodhead J, Hergt J. Iolite: freeware for the visualisation and processing of mass spectrometric data. J Anal At Spectrom. 2011;26:2508–18. https://doi.org/10.1039/C1JA10172B.
38. Hare DJ, Kysenius K, Paul B, Knauer B, Hutchinson RW, O'Connor C, et al. Imaging metals in brain tissue by laser ablation - inductively coupled plasma - mass spectrometry (LA-ICP-MS). J Vis Exp. 2017; https://doi.org/10.3791/55042.

39. Topalä T, Bodoki A, Oprean L, Oprean R. Bovine serum albumin interactions with metal complexes. Clujul Med. 2014;87:215–9. https://doi.org/10.15386/cjmed-357.
40. Michalke B, Nischwitz V. Review on metal speciation analysis in cerebrospinal fluid—current methods and results: a review. Anal Chim Acta. 2010;682:23–36. https://doi.org/10.1016/j.aca.2010.09.054.
41. Nischwitz V, Berthele A, Michalke B. Speciation analysis of selected metals and determination of their total contents in paired serum and cerebrospinal fluid samples: an approach to investigate the permeability of the human blood-cerebrospinal fluid-barrier. Anal Chim Acta. 2008;627:258–69. https://doi.org/10.1016/j.aca.2008.08.018.
42. Roberts BR, Doecke JD, Rembach A, Yévenes FL, Fowler CJ, McLean CA, et al. Rubidium and potassium levels are altered in Alzheimer's disease brain and blood but not in cerebrospinal fluid. Acta Neuropathol Commun. 2016;4:119. https://doi.org/10.1186/s40478-016-0390-8.
43. Hare DJ, Lear J, Bishop D, Beavis A, Doble PA. Protocol for production of matrix-matched brain tissue standards for imaging by laser ablation-inductively coupled plasma- mass spectrometry. Anal Methods. 2013;5:1915–21. https://doi.org/10.1039/C3AY26248K.
44. Christensen R. Log-linear models and logistic regression. 2nd ed. Springer-Verlag; 2006.
45. Saadati N, Abdullah M, Zakaria Z, Sany S, Rezayi M, Hassonizadeh H. Limit of detection and limit of quantification development procedures for organochlorine pesticides analysis in water and sediment matrices. Chem Cent J. 2013;7:1–10. https://doi.org/10.1186/1752-153X-7-63.
46. May TW, Wiedmeyer RH. A table of polyatomic interferences in ICP-MS. At Spectrosc. 1998;19:150–5.
47. Allain P, Jaunault L, Mauras Y, Mermet J, Delaporte T. Signal enhancement of elements due to the presence of carbon-containing compounds in inductively coupled plasma mass spectrometry. Anal Chem. 1991;63:1497–8. https://doi.org/10.1021/ac00014a028.
48. Wiltsche H, Winkler M, Tirk P. Matrix effects of carbon and bromine in inductively coupled plasma optical emission spectrometry. J Anal At Spectrom. 2015;30:2223–34. https://doi.org/10.1039/C5JA00237K.
49. Tanner SD. Space charge in ICP-MS: calculation and implications. Spectrochim Acta Part B At Spectrosc. 1992;47:809–23. https://doi.org/10.1016/0584-8547(92)80076-S.
50. Vanhaecke F, Dams R, Vandecasteele C. 'Zone model' as an explanation for signal behaviour and non-spectral interferences in inductively coupled plasma mass spectrometry. J Anal At Spectrom. 1993;8:433–8. https://doi.org/10.1039/JA9930800433.
51. Frick DA, Günther D. Fundamental studies on the ablation behaviour of carbon in LA-ICP-MS with respect to the suitability as internal standard. J Anal At Spectrom. 2012;27:1294–303. https://doi.org/10.1039/C2JA30072A.
52. Limbeck A, Galler P, Bonta M, Bauer G, Nischkauer W, Vanhaecke F. Recent advances in quantitative LA-ICP-MS analysis: challenges and solutions in the life sciences and environmental chemistry. Anal Bioanal Chem. 2015;407:6593–617. https://doi.org/10.1007/s00216-015-8858-0.
53. Austin C, Fryer F, Lear J, Bishop D, Hare D, Rawling T, et al. Factors affecting internal standard selection for quantitative elemental bio-imaging of soft tissues by LA-ICP-MS. J Anal At Spectrom. 2011;26:1494–501. https://doi.org/10.1039/C0JA00267D.
54. ISO 5725-1: Accuracy (trueness and precision) of measurement methods and results — Part 1: General principles and definitions. Geneva 1994.
55. Roudeau S, Chevreux S, Carmona A, Ortega R. Reduced net charge and heterogeneity of pI isoforms in familial amyotrophic lateral sclerosis mutants of copper/zinc superoxide dismutase. Electrophoresis. 2015;36:2482–8. https://doi.org/10.1002/elps.201500187.
56. Gurney ME. The use of transgenic mouse models of amyotrophic lateral sclerosis in preclinical drug studies. J Neurol Sci. 1997;152 https://doi.org/10.1016/S0022-510X(97)00247-5.
57. Hilton JB, White AR, Crouch PJ. Endogenous Cu in the central nervous system fails to satiate the elevated requirement for Cu in a mutant SOD1 mouse model of ALS. Metallomics. 2016;8:1002–11. https://doi.org/10.1039/c6mt00099a.
58. Roberts BR, Lim NK, McAllum EJ, Donnelly PS, Hare DJ, Doble PA, et al. Oral treatment with Cu^{II}(atsm) increases mutant SOD1 in vivo but protects motor neurons and improves the phenotype of a transgenic mouse model of amyotrophic lateral sclerosis. J Neurosci. 2014;34:8021–31. https://doi.org/10.1523/JNEUROSCI.4196-13.2014.
59. Heffernan AL, Hare DJ. Tracing environmental exposure from neurodevelopment to neurodegeneration. Trends Neurosci. 2018;41:496–501. https://doi.org/10.1016/j.tins.2018.04.005.
60. McIntyre PG. How many drops of CSF is enough? Postgrad Med J. 2007;83:158.
61. Maass F, Michalke B, Leha A, Boerger M, Zerr I, Koch JC, et al. Elemental fingerprint as a cerebrospinal fluid biomarker for the diagnosis of Parkinson's disease. J Neurochem. 2018;145:342–51. https://doi.org/10.1111/jnc.14316.
62. Cardoso B, Hare DJ, Bush A, Li Q-X, Fowler C, Masters C et al. Selenium levels in serum, red blood cells, and cerebrospinal fluid of Alzheimer's disease patients: a report from the Australian Imaging, Biomarker & Lifestyle Flagship Study of Ageing (AIBL). J Alzheimers Dis. 2017;Preprint. doi:https://doi.org/10.3233/JAD-160622.
63. Gerhardsson L, Lundh T, Minthon L, Londos E. Metal concentrations in plasma and cerebrospinal fluid in patients with Alzheimer's disease. Dement Geriatr Cogn Disord. 2008;25:508–15. https://doi.org/10.1159/000129365.
64. Barany E, Bergdahl IA, SchÜTz A, Skerfving S, Oskarsson A. Inductively coupled plasma mass spectrometry for direct multi-element analysis of diluted human blood and serum. J Anal At Spectrom. 1997;12:1005–9. https://doi.org/10.1039/A700904F.
65. Theiner S, Malderen SJM, Acker T, Legin AA, Keppler BK, Vanhaecke F, et al. Fast high-resolution LA-ICP-MS imaging of the distribution of platinum-based anti-cancer compounds in multicellular tumor spheroids. Anal Chem. 2017;89:12641–5. https://doi.org/10.1021/acs.analchem.7b02681.
66. Malderen SJM, Laforce B, Acker T, Nys C, Rijcke M, de Rycke R, et al. Three-dimensional reconstruction of the tissue-specific multielemental distribution within Ceriodaphnia dubia via multimodal registration using laser ablation ICP-mass spectrometry and X-ray spectroscopic techniques. Anal Chem. 2017;89:4161–8. https://doi.org/10.1021/acs.analchem.7b00111.
67. Fittschen UE, Bings NH, Hauschild S, Forster S, Kiera AF, Karavani E, et al. Characteristics of picoliter droplet dried residues as standards for direct analysis techniques. Anal Chem. 2008;80:1967–77. https://doi.org/10.1021/ac702005x.
68. Fittschen UE, Havrilla GJ. Picoliter droplet deposition using a prototype picoliter pipette: control parameters and application in micro X-ray fluorescence. Anal Chem. 2010;82:297–306. https://doi.org/10.1021/ac901979p.